Available online at www.sciencedirect.com
SCIENCE DIRECT
Cement and Concrete Research 35 (2005) 2223–2232
Cement and Concrete Research

An in situ synchrotron energy-dispersive diffraction study of the hydration of oilwell cement systems under high temperature/autoclave conditions up to 130 °C

Sally L. Colston[a], Paul Barnes[a,*], Andrew C. Jupe[a,b], Simon D.M. Jacques[a], Christopher Hall[c,f], Paul Livesey[d], John Dransfield[e], Nicola Meller[c], Geoffrey C. Maitland[f]

[a]*Industrial Materials Group, Department of Crystallography, Birkbeck College, London WC1E 7HX, UK*
[b]*Civil Engineering, Georgia Institute of Technology, Atlanta, Georgia 30332, USA*
[c]*Centre for Materials Science and Engineering and School of Engineering and Electronics, The University of Edinburgh, King's Building, Edinburgh EH9 3JL, UK*
[d]*Castle Cement Ribblesdale Ltd., Clitheroe, Lancashire BB7 4QF, UK*
[e]*38a Tilehouse Green Lane, Knowle, West Midlands B93 9EY, UK*
[f]*Schlumberger Cambridge Research Ltd., High Cross, Madingley Road, Cambridge CB3 0EL, UK*

Received 8 December 2003; accepted 7 September 2004

Abstract

The technique of synchrotron energy dispersive diffraction has been developed for in situ studies of cement hydration under autoclave conditions. This has been applied to oilwell cements hydrating at typical oilwell temperatures up to 130 °C. The results show clearly the detailed interplay between 11 detectable phases, from which a phase transformation scheme has been derived; this illustrates the progression of hydration up to 130 °C for two extreme cases, with and without conservation of water content and autoclave pressure. The monosulphate hydrate phases are found to exhibit different stability bounds, with a surprising sequence of the 14-water, 10-water then 12-water monosulphate as temperature/time increases; the latter form is particularly associated with conditions of water/pressure loss. The effect of retarders on C_3S dissolution and CH formation is negligible above 70 °C, whereas the effect on the calcium sulphoaluminate hydrates is more complex, and possible reasons for this are discussed.

Keywords: Temperature; Hydration products; X-ray diffraction; Oilwell cement; Synchrotron

1. Introduction

Oilwell cements [1–3] are portland cements produced with a low aluminium/iron (A/F) ratio (and hence small or zero C_3A content) to prevent rapid setting under conditions of high temperature/pressure (typically up to 200 °C). In use, they are also strongly retarded by chemical additives. In constructing deep oilwells, cement placement may take many hours so that inadequate retardation can lead to premature setting and catastrophic failure which may require expensive redrilling. The chemistry of hydration in both unretarded and retarded cements under these conditions remains poorly understood largely because of the lack of methods for in situ monitoring of mineralogical transformations under these extreme conditions [4]. The in situ methods described here allow cements to be observed in great details as they hydrate under realistic deep well conditions. The wealth of new hydration behaviour uncovered is remarkable, and this enables us to construct a generic reaction/transformation scheme for cement hydration in this relatively uncharted territory.

* Corresponding author.
E-mail address: p.barnes@bbk.ac.uk (P. Barnes).

0008-8846/$ - see front matter © 2004 Elsevier Ltd. All rights reserved.
doi:10.1016/j.cemconres.2004.09.005

2. In situ energy-dispersive diffraction of cements

Energy-dispersive diffraction (EDD) was first demonstrated in 1968 [5,6], although it was its combination with synchrotron radiation during the mid-1970s [7,8] that transformed it into a versatile technique for in situ studies on crystalline state reactions and transformations. Its application in the area of cement chemistry [9] has proved particularly useful for detecting and monitoring structural changes and transformations in situations where conventional laboratory diffraction methods do not provide the required penetrating radiation (through the sample) nor do they provide sufficient time and space resolutions. Examples of successful expositions using in situ EDD are the capturing of the fleeting intermediate phase during hydration of calcium aluminate cements [10–12] and monitoring the ettringite to monosulphate transformation under various conditions [13]. More recent developments have included the generalisation of EDD to operate simultaneously at different detector angles [14,15] and the exploitation of its spatial resolution to follow hydration fronts in bulk samples (e.g., [16–19]).

The principle of EDD has been described many times (e.g., [20]) and is illustrated schematically in Fig. 1 in the context of these studies: a near-parallel white beam (with, typically, a 20–80 keV usable energy range) from a synchrotron wiggler/multipole magnet is reduced to its final cross-section using precision slits (typically 1000 μm diameter). The beam is then directed through an environmental enclosure into the bulk cement sample from which diffraction occurs according to Bragg's law ($\lambda=2d\ \sin\ \theta$) for the available range of wavelengths λ (0.62 to 0.16 Å for a 20–80 keV source). However, a set of post sample collimators select out just those X-ray photons which have been diffracted at the chosen collimator angles, 2θ (θ being the related angle in Bragg's law). An energy-dispersive detector placed after each collimator determines the energies E [and therefore also the wavelength, inasmuch as λ (Å) $\approx 12.4/E$ (keV)] of the diffracted photons. The multichannel output from an energy-dispersive detector then effectively contains the diffraction pattern but dispersed in energy rather than angle space. Using the reciprocal relationship between λ and E, Bragg's Law can be appropriately recast into the alternative form

$$Ed\sin\theta = hc/2 = \text{constant}\left(\sim 6.2\ \text{keV}\text{Å}\right) \quad (1)$$

where h and c are Planck's constant and the speed of light, respectively, and d is the crystal d-spacing. In the case of a three-angle EDD system, each detector produces an energy-dispersive diffraction pattern appropriate to the 2θ value of its associated collimator/detector; the different θ values for the three collimator/detector combinations result in three different d-spacing ranges for the same intrinsic diffraction pattern. The particular features of EDD are the following:

- It has a fixed geometry, which greatly facilitates the design of the sample environmental cell inasmuch as the entrance/exit beam directions can remain fixed. Furthermore, the lack of moving parts aids the collection of rapid time-resolved diffraction data.
- The white X-ray beam from a synchrotron wiggler magnet is energetic such that it will penetrate through

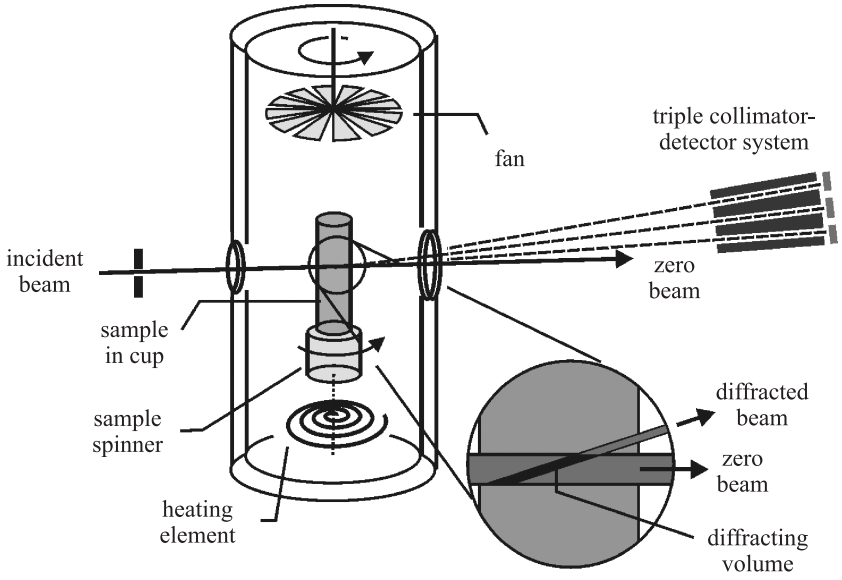

Fig. 1. Schematic of the EDD method operating with an autoclave hydration cell. The incident and (three) diffracted beams define the effective diffracting volume elements (one of which is seen in the exploded view) which is positioned to coincide with a region inside the sample contained within the cylindrical PEEK cell. The PEEK cell sits in a cup which provides (optional) spinning to improve the crystallite orientation sampling. The diffracted beams are defined by the (triple) collimator system, which also houses the energy-dispersive detectors. A regulated hot-air-heater/fan system controls the temperature of the sample cell.

Table 1
List of the most suitable diffraction peaks used in this study for intensity/concentration determinations of the crystalline phases within a hydrating oilwell cement (the abbreviations used in this paper are also indicated)

Mineral/working name	Abbreviation used	Formula	*d*-spacing (Å)	Miller indices
Alite	C_3S	C_3S	3.03	221
Brownmillerite	Bm	C_4AF	7.25	020
Gypsum	gyp	$C\bar{S}H_2$	7.60	020
Portlandite	CH	CH	4.90	001
Hemihydrate/bassanite	hemiH	$C\bar{S}H_{½}$	6.01	200
γ-anhydrite	anH	$C\bar{S}$	6.06	100
α-dicalcium silicate hydrate	C_2SH	α-C_2SH	3.26	122
Ettringite	AFt	$C_3A\ 3C\bar{S}\ H_{32}$	9.72	100
Monosulphate-14	AFm-14	$C_3A\ C\bar{S}\ H_{14}$	9.56	003
Monosulphate-10	AFm-10	$C_3A\ C\bar{S}\ H_{10}$	8.20	003 (assumed)
Monosulphate-12	AFm-12	$C_3A\ C\bar{S}\ H_{12}$	8.75	003

large bulky objects, in extreme cases, up to ~80 mm of concrete [16].
- The diffraction peaks are relatively broad (in energy) which can be problematic if there are many overlapping peaks.

In the present study, it was necessary to build a cement hydration (environmental) cell that was compatible with the X-ray optics of the three-angle EDD system (Fig. 1) and could deliver conditions typical of deep oilwell engineering. Autoclave cells were designed such that it could reliably withstand heating up to 150 °C and 5-bar pressure for bulk cement samples hydrating in autoclave mode; a reusable sealable cell (cylindrical, 8-mm internal diameter) machined from the engineering polymer PEEK was the result. The seals on these cells sometimes fail after repeated use, yet data obtained in such cases are considered useful, although the system no longer remains properly defined. In this context, it is worth noting that variable water/pressure conditions are relevant to oilwell operations inasmuch as bore-holes can develop a range of water/pressure loss regimes by contact through the surrounding porous media. Consequently, some time was set aside for experiments in which water loss was permitted simply as an exploration of the range of results that might occur under such conditions. This revealed some unexpected and interesting comparisons between hydration behaviour under conditions of significant (0.7–7% per hour by weight) and low (0–0.2% per hour by weight) rates of water loss.

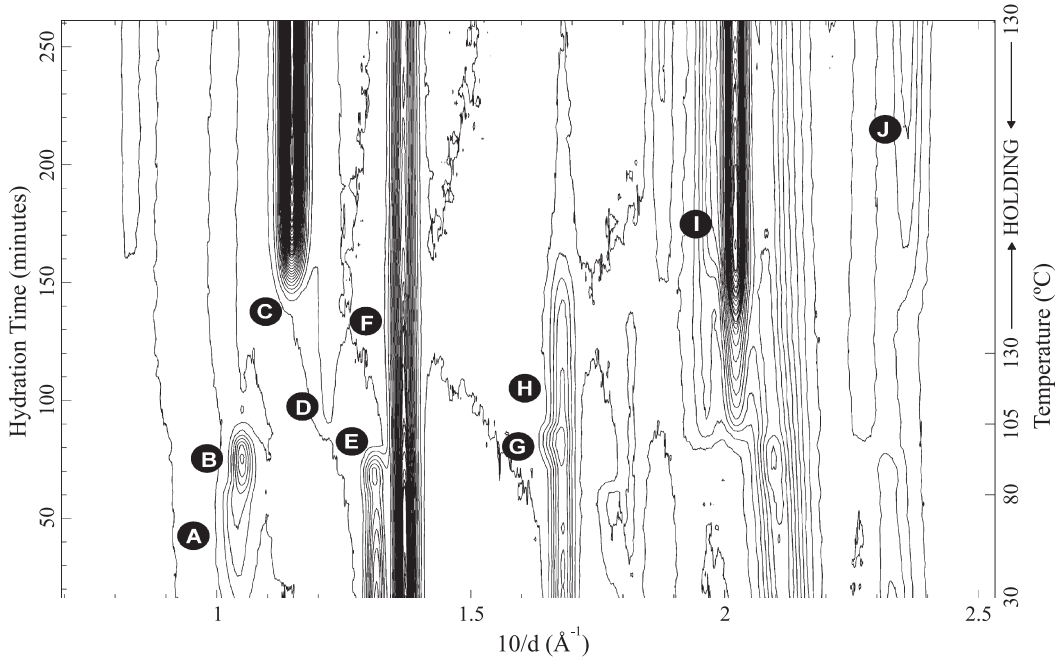

Fig. 2. Example of a 2D contour map of high-quality raw EDD data obtained during an autoclave cement hydration experiment up to 130 °C (the same data set as in Fig. 3a). Such diffraction patterns are dispersed in one of the dimensions, in energy (keV) or the equivalent in reciprocal space terms [10/*d* (Å)] as shown. The other dimension resolves the patterns in time and temperature. Some examples of identification are indicated by lettering close to the appropriate diffraction peak: A=ettringite, B=14-water monosulphate, C=12-water monosulphate, D=10-water monosulphate, E=gypsum, F=brownmillerite, G=γ-anhydrite, H=hemihydrate, I=calcium hydroxide, J=α-C_2SH.

Diffraction patterns from portland cements are notoriously complex, and it might seem at first, given the broad diffraction peaks inherent with EDD, that assignment of cement phases within a changing (hydrating) system could be problematic. However, the outcomes from many in situ hydration experiments have provided sufficient familiarity with the characteristic ED diffraction patterns that phase assignment can be performed unambiguously and suitable (nonoverlapping) peak(s) can be identified for the purpose of quantitative analysis (concentration plots); the only exception to this are the γ-anhydrite and hemihydrate phases which have closely spaced diagnostic peaks with the result that there is some unavoidable correlation between the determined concentrations of these two particular phases. In the case of the monosulphate phases, the 14-water [21] and 10-water [22] forms can be distinguished from the more common 12-water form by the long basal *d*-spacings. Table 1 lists the most useful ED diffraction peaks used for the main phases and their abbreviated names used in the figures.

The time-resolved EDD data comprise a series of diffraction patterns representing the changing composition of the hydrating sample at different times; the time intervals between each data set, often referred to as the time resolution, were set for these experiments to be either 5 (medium time resolution) or 25 min (low time resolution). Such time-resolved series can be displayed as a three-dimensional surface or two-dimensional contour map of the raw data; an example of the latter is given in Fig. 2. Although these forms are visually informative, it is customary to convert such data to more quantitative representations by fitting Gaussian profiles to the diagnostic diffraction peak(s) and determining the area of each peak, which is then taken to be proportional to its intensity and to the weight fraction of the phase it represents. After these data are corrected for the time variations in the synchrotron beam current (beam decay), the resulting plots (e.g., Fig. 3) represent relative changes with time in concentration of each phase inasmuch as the total elemental composition is conserved (with low water/pressure loss experiments), and

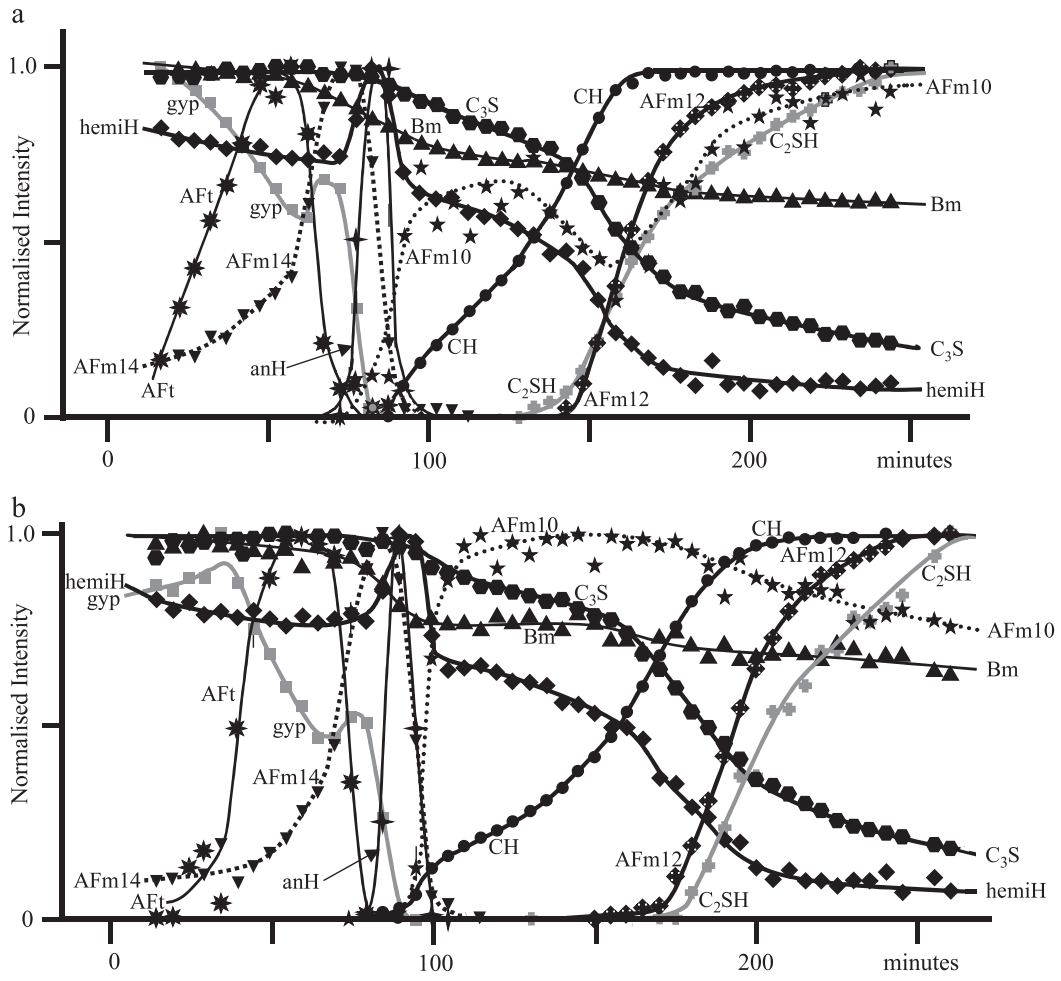

Fig. 3. Time-resolved phase concentration versus time plots for hydration experiments at 130 °C. Each plot is normalised so that its maximum is unity (consequently, the AFm-10 plots appear very noisy inasmuch as their absolute levels of concentration are relatively low): (a) oilwell cement, hydrating with a 0.7% per hour water loss; (b) as in panel (a) but with 0.1% phosphonate retarder added and a 0.9%-per-hour water loss. Clearly, the retarder makes little difference at these temperatures. No less than 11 separate phases are monitored (the key to the phases is given in Table 1).

the X-ray absorption remains effectively constant once the cement has settled inside the autoclave cell. In order to obtain absolute concentrations, one would need to normalise the data against samples of known composition; however, valuable information can still be gleaned from relative concentrations inasmuch as their variation with time, simultaneously or sequentially for two or more phases, enables one to infer the key interactions between the various phases. Many examples are presented below. They represent the most novel part of this study as there is no other available experimental way of extracting such detailed correlations between the appearance and disappearance of mineral phases during hydration.

3. Results and discussion

In the following in situ experiments, a Dyckerhoff API Class G cement (A/F=0.83; surface area=310 m^2/kg; free lime=0.5%; alkalis=0.55% Na_2O equivalent) was chosen as a representative oilwell cement, calcium gluconate and sodium phosphonate (pentasodium salt of ethylenediamine-tetramethylenephosphonic acid supplied by Monsanto under the name Dequest 2046) were selected as example retarders. These compounds are chemically dissimilar and may well retard hydration by different mechanisms. Silica flour was also included as a commonly used additive for the prevention of strength loss at high temperature [1]. A water/cement ratio of 0.4 (by weight) was used for all the experiments in this study. Four temperature profiles were chosen, in which the sample is heated from near-ambient (20–30 °C) to the set temperature on a linear temperature ramp over 2 h, as the target temperature profile, and thereafter held at the set (top) temperature. These profiles are referred to as 30, 30–70, 30–100 and 30–130 °C, respectively. The actual sample temperatures were found to be within a few degrees of these target profiles, except near the end of the ramp towards the highest temperature, 130 °C, for which the time-lag could be up to 10 min. Once the set temperatures were achieved, they were maintained within ±1°C. Hydration within the four main temperature profiles was studied both without (the "control") and with the two prototype additives and with/without water/pressure loss through the sample seal. The control cement is considered first.

3.1. Control oilwell cement (no additives)

The hydration behaviour of the oilwell cements was investigated in situ as the temperature was ramped between 30 and 130 °C. Comparative data for the cases of negligible and significant water/pressure loss were obtained for three elevated temperatures (70, 100 and 130 °C), and these are given in Table 2 together with the ambient control data. They show how the calcium hydroxide growth is brought forward with increasing temperature, this acceleration being moderated and more unpredictable when there is significant loss of water/pressure, except that, at 130 °C, the trend changes (this exception is considered further at a later point). Similar observations can be made for the other events listed (loss of the main sulphate phases).

Increasing the temperature brings about more complex hydration scenarios. This is very apparent from Fig. 3 which superimposes the progress of no less than 11 separate phases, and therefore some breakdown of the overall picture into component events is necessary. In some cases, it is possible to identify specific events which cause the hydration paths to diverge. One such example is the transition of ettringite to a primary monosulphate hydrate which has been identified here unambiguously as the 14-water form, in keeping with the observations of Kuzel [21]. This transition is not observed at 30 °C but is clearly seen at 70 °C and higher temperatures (e.g., Fig. 3). However, it appears that not all the 14-water monosulphate originates from ettringite but that there is also a prior contribution from the combination of gypsum and brownmillerite, as indicated by two differently characterised growth regions. The first steadier region corresponds with the steady loss of gypsum and brownmillerite, while the second more rapid region coincides with the rapid loss of ettringite. As the temperature rises further (100 and 130 °C), the greater stability of the 10-water over the 14-water monosulphate becomes influential, and an interplay between these two phases and brownmillerite (loss)/CH (production) becomes apparent.

Table 2
Comparative data on the times (to nearest 5 min) and temperatures at which calcium hydroxide (CH) starts to form, and the ettringite, gypsum and 14-water monosulphate are completely consumed; "disappearance" is taken to be the point when a diffraction peak becomes indistinguishable from the background

Temperature profile; water/pressure loss	*N*	CH appears; time temperature	AFt→0; time temperature	Gypsum→0; time temperature	AFm_{14}→0; time temperature
30 °C; low	1	320 min 30 °C	N/A	630^+ min 30 °C	N/A
30–70 °C; low	2	140 min 70 °C	215 min 70 °C	195 min. 70 °C	300 min 70 °C
30–70 °C; significant	3	240 min 70 °C	300 min 70 °C	250 min 70 °C	600^+ min 70 °C
30–100 °C; low	1	120 min 95 °C	200 min 100 °C	200 min 100 °C	200 min 100 °C
30–100 °C; significant	2	180 min 98 °C	130 min 99 °C	175 min 98 °C	220 min 98 °C
30–130 °C; low	1	85 min 95 °C	82 min 90 °C	83 min 95 °C	95 min 100 °C
30–130 °C; significant	3	170 min 130 °C	120 min 130 °C	170 min 130 °C	195 min 130 °C

A plus sign indicates that the event had not been observed at the time of the end of the experiment. The data cover various temperature profiles, both with and without significant water/pressure loss (the number of successful experiments for each entry is given as "*N*").

The hydration behaviour becomes more divergent with water/pressure loss at the highest temperatures, and this is discussed later. First, we need to summarise the basic events observed for the four main temperature regimes studied:

- 30 °C: the obvious events are the steady growth in ettringite and standard hydration of C_3S to CH/C–S–H, the reaction of brownmillerite being very slow;
- 30–70 °C: the C_3S to CH/C–S–H hydration is accelerated. The brownmillerite reaction speeds up significantly during the production of CH and 14-water monosulphate. The ettringite transforms to 14-water monosulphate. Gypsum reaction is complete;
- 30–100 °C: the 14-water monosulphate structure breaks up. A relatively small amount of 10-water monosulphate forms and appears to remain stable;
- 30–130 °C: the hydration behaviour changes markedly with water/pressure loss, in particular exhibiting late growth of stable 12-water monosulphate and α-C_2SH.

As already stated, the richest variety of events appears at the highest temperature for the cases of significant water/pressure loss: indeed Fig. 3 probably represents the first occasion that all three hydrates (14-, 10-, then 12-water) of the monosulphate are explicitly recorded during one experimental sequence and, even then, in a surprising nonmonotonic order of water content. It is observed that the decomposition temperature of ettringite drops with decreasing pressure, in common with Ogawa and Roy's observation [23] on pure systems, the corresponding dependence on water vapour pressure having been studied by Zhou and Glasser [24]. It is instructive to examine the water/pressure loss regime in more details as an illustration of the variety of hydration reactions that can be observed up to 130 °C. The great advantage of time-resolved in situ data such as these is that interphase relationships can be interpreted from the coincidences between changes in concentration variation of two or more phases. We list the main examples relating to Fig. 3: the observation is given in ordinary type case, and the resulting deduction is shown in italics, the time/temperature values are included only to give an approximate indication of when each event occurs; for ease of perception, the relevant observations are extracted from Fig. 3 and shown schematically in Fig. 4:

- 76 °C, 65 min (Fig. 4a): As discussed above, the production of 14-water monosulphate (AFm-14) appears to be bimodal: Initially, both ettringite (AFt) and AFm grow together, but then the AFm growth accelerates sharply once the AFt begins to decompose. This also coincides with an upward "blip" during gypsum consumption. The brownmillerite consumption rate also increases from this point: *Initially, the 14-water monosulphate forms from brownmillerite and gypsum, but its growth accelerates sharply once the ettringite decomposes and provides an alternative sulphoaluminate source to the point that excess sulphate is thrown out and temporarily reforms as additional gypsum.*
- 88 °C, 80 min (Fig. 4b): *The continued loss of gypsum (after its upward blip) and the breakup of AFm-14 coincide with the rapid production of calcium sulphate hemihydrate (bassanite). There is also a small amount of anhydrite produced, but peak overlap prevents accurate monitoring of this minor phase: The dissolution/decomposition of gypsum and breakup of 14-water monosulphate cause sulphate to be thrown out in the form of hemihydrate*.
- 96 °C, 90 min (Fig. 4c): The AFm-10 growth coincides with a rapid loss of hemihydrate, the gypsum having already been completely depleted earlier, and the brownmillerite (the only aluminate source) consumption

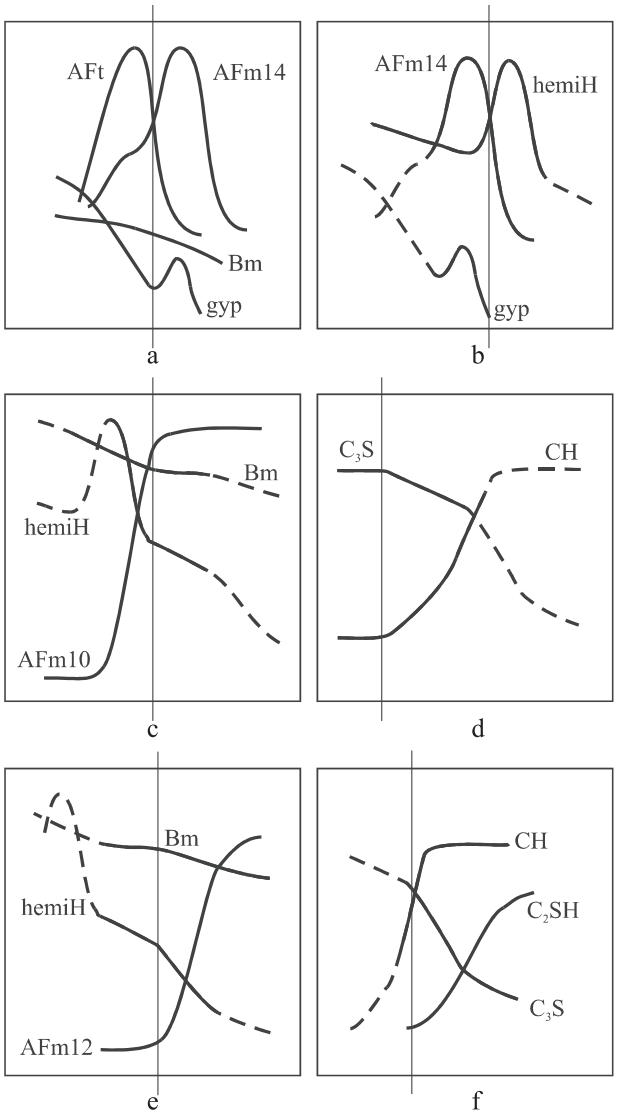

Fig. 4. Schematic sections (a–f) extracted from Fig. 3 to illustrate key interrelationships between the various phases (key as in Fig. 3). Each plot is a schematic representation of relative changes in concentration versus time for the relevant phases. The significant "turning point" is marked by a thin vertical line.

slows down once the AFm-10 is formed: *A small amount of 10-water monosulphate is formed, not directly from the break-up of 14-water monosulphate but rather indirectly from the intermediate hemihydrate which seems to have acted as a temporary storage of sulphate until it combines with some of the brownmillerite*.

- 84–130 °C, 75–150 min: The sulphate content released corresponding to the complete consumption of gypsum, breakup of AFm-14 and hemihydrate cannot be fully accounted for by crystalline sulphate phases inasmuch as the quantity of AFm-10 formed is small, and the AFm-12 production does not start until considerably later (~150 min): *Some of the sulphate content released by the breakup of the gypsum, 14-water monosulphate and hemihydrate must (temporarily at least) be stored in an amorphous form. This ties in with reports in the literature (e.g., [25,26]) of sulphate groups becoming dispersed within the C–S–H amorphous phase*.
- 92 °C, 85 min (Fig. 4d): The commencement of CH formation coincides with an increase in the rate of C_3S consumption. *The end of the well-known cement induction period is signalled by the start of CH formation and an increase in the C_3S consumption rate*.
- 130 °C, 145 min (Fig. 4e): The formation of AFm-12 coincides with a slight increase in the brownmillerite consumption rate and a more noticeable increase in consumption of the hemihydrate, which becomes mostly exhausted (there is also an increase in the C_3S consumption rate): *12-water monosulphate is formed, similarly to the previous 10-water monosulphate, from brownmillerite and hemihydrate, although additional sulphate dispersed in the C–S–H (vide supra) might also be available (the C_3S consumption is not directly related to AFm-12; see the next event below)*.
- 130 °C, 145 min (Fig. 4f): The formation of α-C_2SH coincides with the increase in consumption rate of C_3S, but notably, the CH appears to remain constant: *The high-temperature crystalline hydrate α-C_2SH is formed from C_3S.*
- 130 °C, 145 min: There is an obvious coincidence between the two previous events at high temperatures with water/pressure loss: *A plausible mechanism is that, under conditions of combined high temperature and water/pressure loss, the C–S–H phase becomes partly destabilised so that some C–S–H and locally dispersed–$\overline{S}$ are simultaneously released and able to nucleate growth of both α-C_2SH and 12-water monosulphate*.

All these links and deductions have been incorporated into a schematic figure (Fig. 5), depicting the overall transformation scheme for a hydrating oilwell cement when (a) water/pressure loss is zero/negligible and (b) when water/pressure loss is considerable. Although some temperature/time indications are included from the specific data sets with Fig. 3, the diagram is intended to be generic for high temperature hydration, generally, the latter stage being more specific to systems experiencing water/pressure loss. The overall level of new detail is remarkable and stands as a tribute to the power of in situ studies. Similar detail is apparent in a companion study [28] of brownmillerite/gypsum hydration.

3.2. Oilwell cement hydration with additives

Two prototype retarders have been used in this study, calcium gluconate and sodium phosphonate, the range of dosages 0.1–0.2% (by weight) being typical of industrial practice. One might at first perceive a relatively simple picture concerning the effect of these retarders if one were to restrict observations to the main crystalline components C_3S and CH: Table 3 shows that, at ambient temperatures, the effect of retarders is to decrease the rate of C_3S dissolution and to delay the onset of CH growth from about 320 min to times beyond the normal duration of the experiment (i.e., >600 min); at 70 °C, this delay is less pronounced (200 to 385+ min), and, at higher temperatures (100 and 130 °C), the difference is negligible (it is an oddity that the shortest onset times occur at 100 rather than 130 °C). Furthermore, the dosage dependence appears to be normal, the degree of delay increasing steadily with dosage. However, if one examines the behaviour of other hydration components (ettringite, gypsum, AFm-14, AFm-10, AFm-12 and α-C_2SH), the trends are less clear. Table 3 shows that gypsum dissolution is either delayed or unaltered by retarders up to 70 °C but accelerated at higher temperatures. The behaviours of the three monosulphate phases are very varied, AFm-14 formation being suppressed by calcium gluconate and delayed by sodium phosphonate, AFm-10 (100, 130 °C) being slightly accelerated with Ca gluconate and significantly accelerated by sodium phosphonate and, notably, AFm-12 forming at temperatures as low as 100 °C with Ca gluconate. Such differing behaviour must be due in part to divergence of reaction pathways early in the hydration process, and early ettringite formation is obviously a significant factor given its sensitivity to additives and its subsequent transformation to the first monosulphate, AFm-14: Table 3 also gives an indication of the quantity of ettringite being produced within each field (compared to the control), the general trend being towards a reduction but with the calcium gluconate being far more effective at reducing the ettringite formed, particularly at 100 °C or above. This is particularly interesting in that phosphonate retarders are believed to interact strongly with the surface of ettringite crystallites, with possible consequences of modified crystal growth. Information on modified crystallite shape cannot realistically be gleaned from EDD patterns due to the broadness of the diffraction peaks. By contrast, a gluconate retarder is believed to act as an ion complexer, and, on this basis, one might surmise that the very significant reduction in ettringite stems from some interference between the gluconate and the gypsum calcium cations, which normally feed the ettringite production.

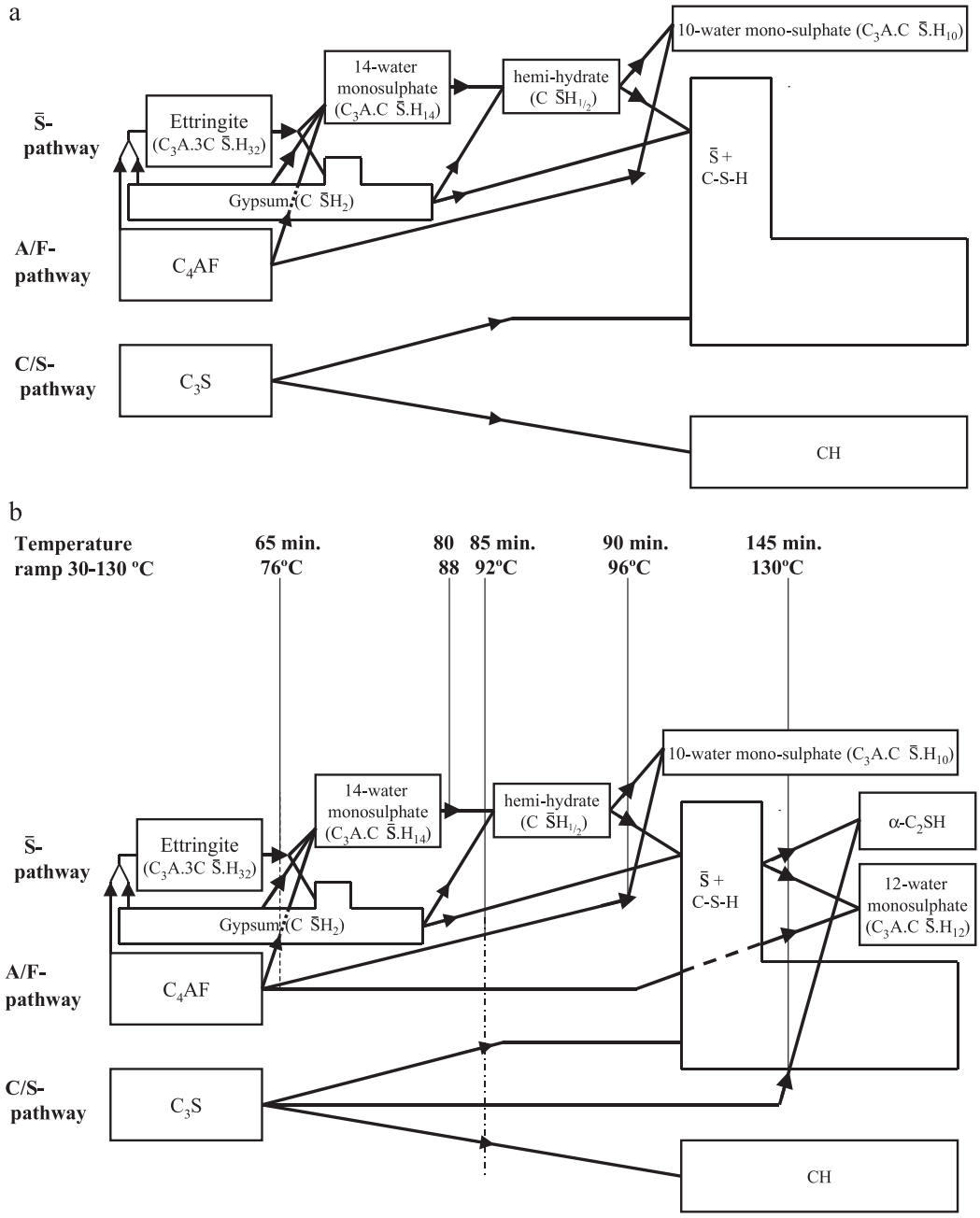

Fig. 5. Schematic transformation pathways derived from the data such as those presented in Figs. 3 and 4, organised according to sources of sulphate ($\bar{S}$), alumino–ferrite (A/F) and silicate (S). The usual solid solution substitutions (e.g., Al/Fe) are assumed: (a) with zero or negligible water/pressure loss, (b) with significant water/pressure loss. The γ-anhydrite formation is not shown separately as it can be considered as a correlated subcomponent, i.e., part of the hemihydrate production box. The temperature and time markings given in Fig. 5b are as for Fig. 3a and are only included to give an approximate indication of when each event occurs.

Subsequent observation of the ettringite to monosulphate transformation (AFt→AFm-14) then reflects upon the quantity of ettringite that has been formed in the first place and is therefore available for transformation coupled with the increasing slowness of this transformation at or below 70 °C [13,27,28]. Another notable feature is that the formation of 12-water monosulphate and α-C_2SH (AFm-12/α-C_2SH), which in Eq. (1) was linked to destabilisation by high temperature and water/pressure loss, occurs as low as 100 °C, even with negligible water/pressure loss in the case of the gluconate retarder. No obvious reason can, at present, be offered for this except the idea that somehow, in supressing the ettringite and AFm-14 production, the gluconate additive also induces a less robust C–S–H microstructure, which is then more easily destabilised.

The remaining observation on additives, not covered in Table 3, concerns the addition of silica flour (50% by weight to cement). This procedure is commonly used in oilwell

Table 3
Comparative data on phase evolution for the control (OPC), control with 0.1 (or 0.2*) wt.% calcium gluconate and control with 0.1 (or 0.2*) wt.% sodium phosphonate for autoclave hydration at temperatures ramped from 30 to 70, 100 and 130 °C over 2 h

Event		Control OPC (min)	OPC+Ca-gluconate (min)	OPC+Na-phosphonate (min)
CH formation	30 °C	320	600+	600+
	70 °C	200	385+	385+
	100 °C	115–180	104	160–315*
	130 °C	167	170	155
Ettringite growth	30 °C	Control	Low	≈Control
	70 °C	Control	Fairly low	≈Control
	100 °C	Control	Zero	Fairly low
	130 °C	Control	Very low	≈Control
Gypsum dissolution	30 °C	600+	600+	600+
	70 °C	220	385	385+
	100 °C	200	160	140–335*
	130 °C	193	180	150
AFt→AFm-14	30 °C	NO	NO	NO
	70 °C	360+	NO	385+
	100 °C	170	NO	150–495*
	130 °C	166	180	210–500*
AFm-10 growth	30 °C	NO	NO	NO
	70 °C	NO	NO	NO
	100 °C	170	162	100–305*
	130 °C	191	180	87–145*
AFm-12/α-C_2SH	30 °C	NO	NO	NO
	70 °C	NO	NO	NO
	100 °C	NO	NO	NO
	130 °C	YES	YES	YES

CH formation denotes the time at which calcium hydroxide (CH) starts to form. Ettringite formation compares, at a suitable reference time, the quantity of ettringite produced to that from the control, the levels being ca equal (≈control), fairly low (~50%), low (20–35%), very low (<15%) and zero (not measurable). Gypsum dissolution gives the times at which the gypsum peak disappears. AFt→AFm-14 signifies the time at which the ettringite disappears during its decomposition to 14-water monosulphate. AFm-10 growth signifies the time at which the 10-water-monosulphate starts to grow. AFm-12/α-C_2SH indicates whether or not 12-water monosulphate and α-C_2SH develop. YES/NO signify that the event did/did not occur under the given conditions. A plus sign indicates that the event had not been observed at the time of the end of the experiment, an asterisk denotes that the value is found to be dosage-dependent between 0.1% and 0.2%. Because of the very different scenarios encompassed, the data are only truly comparable across each individual row.

operations to prevent strength regression and is believed to modify the formation of high-temperature hydrates. This addition was studied using both true autoclave and non-autoclave (water/pressure loss) conditions. The resultant data show that crystalline α-C_2SH is suppressed by the increased Si/Ca ratio from silica addition, although, interestingly, no other crystalline C–S–H phases are found.

4. Conclusions

Synchrotron energy dispersive in situ diffraction is a powerful tool for studying the hydration behaviour of cements at elevated temperature and pressure. In this study, the behaviour of oilwell cements has been examined for a variety of temperature/pressure conditions, with and without two example retarders. The level of detail concerning the behaviour (growth, decay) and interdependency of the crystalline phases is remarkable, enabling some firm conclusions to be drawn concerning the hydration pathways in spite of the complex nature of the system. Particular highlights are the elucidation of events involved in the interplay between the sulphate phases (gypsum, ettringite, hemihydrate and AFm-*N*, *N*=10,14) and the mode of destabilisation of the whole system under nonequilibrium (water/pressure loss) conditions. This latter regime uncovers a somewhat surprising formation sequence and partial coexistence of three monosulphate phases (in order: AFm-14, AFm-10, AFm-12) and the high-temperature crystalline hydrate α-C_2SH. These events are in turn influenced by the addition of retarders: at lower temperatures, it is mainly the rates of C_3S dissolution and CH formation that are altered; at higher temperatures, the retarders have little effect on these two issues, instead, the growth kinetics of the sulphate-containing phases is markedly changed. Although only two retarders were examined, their behaviour and modes of action are shown to be different and suggest that this EDD methodology could be a valuable tool for identifying different modes of cement hydration across a range of additives.

Acknowledgements

The authors wish to acknowledge essential funding by the EPSRC, Castle Cement, Schlumberger Cambridge Research and Fosroc International, the award of synchrotron beamtime at the Daresbury SRS synchrotron and the help of

their staff, the workshop effort of Mr. Paul Stukas and finally the advice of Prof. John Bensted.

References

[1] E. Nelson (Ed.), Well Cementing, Schlumberger Educational Services, Sugar Land, Texas, 1990.
[2] J. Bensted, in: P.C. Hewlett (Ed.), Lea's Chemistry of Cement and Concrete, Butterworth-Heinemann, Oxford, 1998, pp. 779–835.
[3] J. Bensted, Developments with oilwell cements, in: J. Bensted, P. Barnes (Eds.), Structure and Performance of Cements, Spon Press, London, 2002, pp. 237–252.
[4] K. Luke, C. Hall, T. Jones, P. Barnes, X. Turrillas, A. Lewis, New techniques for monitoring cement hydration under simulated well conditions, SPE International Symposium on Oilfield Chemistry, San Antonio, TX, SPE 28958, 1995, pp. 137–144.
[5] B.C. Geissen, G.E. Gordon, X-ray diffraction: new high speed technique based on X-ray spectrography, Science 159 (1968) 973–975.
[6] B. Buras, J. Chwaszczewska, S. Szarras, Z. Szmid, Fixed angle scattering (FAS) method for X-ray crystal structure analysis, Inst. Nucl. Res. (Warsaw) Rep. No. 894/II/PS (1968).
[7] J. Bordas, A.M. Glazer, C.J. Howard, A.J. Bourdillon, Energy-dispersive diffraction from polycrystalline materials using synchrotron radiation, Philos. Mag. 35 (1977) 311.
[8] B. Buras, J. Staun Olsen, L. Gerward, X-ray energy-dispersive powder diffractometry using synchrotron radiation, Nucl. Instrum. Methods 135 (1976) 193–195.
[9] P. Barnes, S.L. Colston, A.C. Jupe, S.D.M. Jacques, M. Attfield, R. Pisula, S. Morgan, C. Hall, P. Livesey, S. Lunt, The use of synchrotron sources in the study of cement materials, in: J. Bensted, P. Barnes (Eds.), Structure and Performance of Cements, Spon Press, London, 2002, pp. 477–499.
[10] S. Rashid, P. Barnes, X. Turrillas, The rapid conversion of high alumina cement hydrates, as revealed by synchrotron energy dispersive diffraction, Adv. Cem. Res. 4 (1992) 61–67.
[11] A.C. Jupe, X. Turrillas, P. Barnes, S.L. Colston, C. Hall, D. Häusermann, M. Hanfland, Fast in situ X-ray diffraction studies of chemical reactions: a synchrotron view of the hydration of tricalcium aluminate, Phys. Rev., B 53 (1996) 14697–14700.
[12] S. Rashid, P. Barnes, J. Bensted, X. Turrillas, Conversion of calcium aluminate cement hydrates re-examined with synchrotron energy-dispersive diffraction, J. Mater. Sci. Lett. 13 (1994) 1232–1234.
[13] P. Barnes, X. Turrillas, A.C. Jupe, S.L. Colston, D. O'Connor, R.J. Cernik, P. Livesey, C. Hall, D. Bates, R. Dennis, Applied crystallography solutions to problems in industrial solid state chemistry: case examples with ceramics, cements and zeolites, J. Chem. Soc., Faraday Trans. 92 (1996) 2187–2196.
[14] P. Barnes, A.C. Jupe, S.L. Colston, S.D.M. Jacques, A. Grant, T. Rathbone, M. Miller, S.M. Clark, R.J. Cernik, A new three-angle energy-dispersive diffractometer, Nucl. Instrum. Methods Phys. Res., B Beam Interact. Mater. Atoms 134 (1998) 310–313.
[15] S.L. Colston, S.D.M. Jacques, P. Barnes, A.C. Jupe, C. Hall, In-situ hydration studies using multi-angle energy-dispersive diffraction, J. Synchrotron Radiat. 5 (1998) 112–117.
[16] C. Hall, S.L. Colston, A.C. Jupe, S.D.M. Jacques, R. Livingston, E-S. Ramadan, P. Barnes, Non-destructive tomographic energy-dispersive diffraction imaging (TEDDI) of the interior of bulk concrete, Cem. Concr. Res. 30 (2000) 491–495.
[17] P. Barnes, S.L. Colston, B. Craster, C. Hall, A.C. Jupe, S.D.M. Jacques, J.K. Cockcroft, S. Morgan, M. Johnson, D. O'Connor, M. Bellotto, Time- and space-resolved dynamic studies on ceramic and cementitious materials, J. Synchrotron Radiat. 7 (2000) 117–177.
[18] P. Barnes, S.L. Colston, A.C. Jupe, S.D.M. Jacques, M. Attfield, S.P. Bailey, R. Pisula, C. Hall, P. Livesey, The use of a variety of synchrotron techniques in the study of cementitious materials, Mater. Res. Soc. Symp. Proc. 678 (2001) EE5.4.1–EE5.4.18.
[19] A.P. Wilkinson, C. Lind, S.R. Stock, K.E. Kurtis, N. Naik, D.R. Haeffner, P.L. Lee, Mapping the distribution of corrosion products in cement exposed to sulfate using energy dispersive X-ray diffraction, Mater. Res. Soc. Symp. Proc. 678 (2001) EE5.3.1–EE5.3.6.
[20] D. Häusermann, P. Barnes, Energy-dispersive diffraction with synchrotron radiation: optimisation of the technique for dynamic studies of transformations, Phase Transit. 39 (1992) 99–115.
[21] H.-J. Kuzel, Initial hydration reactions and mechanisms of delayed ettringite formation in Portland cements, Cem. Concr. Compos. 18 (1996) 195–203.
[22] K.L. Scrivener, H.F.W. Taylor, Delayed ettringite formation: a microstructural and microanalytical study, Adv. Cem. Res. 5 (1993) 139–146.
[23] K. Ogawa, D.M. Roy, $C_4A_3\overline{S}$ hydration ettringite formation, and its expansion mechanism: I. expansion; ettringite stability, Cem. Concr. Res. 11 (1981) 741–750.
[24] Q. Zhou, F.P. Glasser, Thermal stability and decomposition mechanisms of ettringite at <120 °C, Cem. Concr. Res. 31 (2001) 1333–1339.
[25] I. Odler, Interaction between gypsum and the CSH phase formed in C_3S hydration, Proc. 7th Int. Cong. Chem. Cem. 4 (1980) 493–495.
[26] Yan Fu, Ping Gu, Ping Xie, J.J. Beaudoin, A kinetic study of delayed ettringite formation in hydrated Portland cement paste, Cem. Concr. Res. 25 (1995) 63–70.
[27] C. Hall, P. Barnes, A. Billimore, A.C. Jupe, X. Turrillas, Thermal decomposition of ettringite $Ca_6[Al(OH)_6]_2(SO_4)_3 \cdot 26H_2O$, J. Chem. Soc., Faraday Trans. 92 (1996) 2125–2129.
[28] N. Meller, C. Hall, A.C. Jupe, S.L. Colston, S.D.M. Jacques, P. Barnes, Time resolved studies of the hydration of brownmillerite with and without gypsum: a synchrotron diffraction study at ambient and elevated temperature, J. Mater. Chem. 14 (2004) 428–435.